Editors' Suggestion | Featured in Physics

Measurement of the ^{229}Th Isomer Energy with a Magnetic Microcalorimeter

Tomas Sikorsky,[1,2,*] Jeschua Geist,[1,*] Daniel Hengstler,[1] Sebastian Kempf,[1] Loredana Gastaldo,[1] Christian Enss,[1] Christoph Mokry,[3,4] Jörg Runke,[3,5] Christoph E. Düllmann,[3,4,5] Peter Wobrauschek,[2] Kjeld Beeks,[2] Veronika Rosecker,[2] Johannes H. Sterba,[2] Georgy Kazakov,[2] Thorsten Schumm,[2] and Andreas Fleischmann[1]

[1]*Kirchhoff-Institute for Physics, Heidelberg University, INF 227, 69120 Heidelberg, Germany*
[2]*Institute for Atomic and Subatomic Physics, TU Wien, Stadionallee 2, 1020 Vienna, Austria*
[3]*Department of Chemistry - TRIGA Site, Johannes Gutenberg University, Fritz-Strassmann-Weg 2, 55128 Mainz, Germany*
[4]*SHE Chemistry, Helmholtz Institute Mainz, Staudingerweg 18, 55128 Mainz, Germany*
[5]*SHE Chemistry, GSI Helmholtzzentrum für Schwerionenforschung mbH, Planckstr. 1, 64291 Darmstadt, Germany*

(Received 28 May 2020; revised 8 July 2020; accepted 20 August 2020; published 28 September 2020)

We present a measurement of the low-energy (0–60 keV) γ-ray spectrum produced in the α decay of ^{233}U using a dedicated cryogenic magnetic microcalorimeter. The energy resolution of ~10 eV, together with exceptional gain linearity, allows us to determine the energy of the low-lying isomeric state in ^{229}Th using four complementary evaluation schemes. The most precise scheme determines the ^{229}Th isomer energy to be 8.10(17) eV, corresponding to 153.1(32) nm, superseding in precision previous values based on γ spectroscopy, and agreeing with a recent measurement based on internal conversion electrons. We also measure branching ratios of the relevant excited states to be $b_{29} = 9.3(6)\%$ and $b_{42} < 0.7\%$.

DOI: 10.1103/PhysRevLett.125.142503

The low-energy metastable isomeric state in ^{229}Th (^{229m}Th) has fascinated researchers over the past 40 years [1]. It is expected to have an excitation energy of ~8 eV, making it the only nuclear state accessible to laser manipulation known so far. Optical excitation of the ^{229}Th nucleus would allow us to transfer the precision of laser spectroscopy to nuclear structure analysis [2]. A plethora of applications and investigations have been proposed for the ^{229m}Th state, ranging from a nuclear gamma laser [3], a highly accurate, and stable ion nuclear clock [4,5] to a compact solid-state nuclear clock [4,6,7]. Such clocks would allow to attain a new level of precision for probes of fundamental physics, e.g., a variation of fundamental constants [8–10], search for dark matter [11,12] or as a gravitational wave detector [13]. They can be used in different applications, such as geodesy [14] or satellite-based navigation [15].

Despite considerable efforts, neither the resonant optical excitation of ^{229m}Th from the nuclear ground state nor the emission of fluorescence photons in radiative decay has been observed [16]. Several recent attempts to excite the nucleus using broadband synchrotron radiation failed to detect a signal [17–19]. All currently available information about the existence [20,21], the energy [22–25], or lifetime [26] of the isomer is derived from experiments where the ^{229}Th isomer is produced in α decay of ^{233}U, or through the x-ray pumping of the second excited nuclear state [27]. A next step on the way toward the nuclear clock is the direct laser-based excitation of the isomeric state. For this, precise knowledge on the excitation energy is needed, as state-of-the-art four-wave mixing laser systems suitable to scan in this energy region and hence identify the transition typically cover a wavelength range of only a few nanometers.

The existence of a low-lying isomeric state in ^{229}Th was deduced in 1976 from analysis of a γ-ray spectrum associated with α decay of ^{233}U [28]. Refined measurements of the same spectrum performed in the early 90s with different Ge and Si(Li) detectors, whose energy resolution was about several hundreds of eV, determined the isomer energy to be 3.5(10) eV [29]. Reanalysis of these spectra gave 5.5(10) eV [30]. Later, a more precise measurement using a NASA x-ray microcalorimeter spectrometer with an energy resolution of ~30 eV measured an isomer energy of 7.8(5) eV, shifting the transition into the vacuum ultraviolet region [23,24]. Recently, another calorimetric experiment with ~40 eV energy resolution reported the isomer energy to be 8.30(92) eV [25], consistent with the previous result but not improving upon the uncertainty.

The ^{229m}Th state was also studied by direct spectroscopy of recoil ions emerging from a ^{233}U source. The ^{233}U → ^{229}Th decay populates the ^{229m}Th state with a 2% probability [31]. Thorium ions were slowed down in a buffer gas and selectively extracted in a quadrupole mass separator [21]. Nuclear magnetic dipole and electric quadrupole moments of the ^{229m}Th isomer have been deduced from laser spectroscopy data [31]. The lifetime of the ^{229m}Th state for atoms deposited onto the MCP detector surface has been measured [26]. Finally, an isomer energy of 8.28(17) eV has been determined by spectroscopy of the internal conversion electrons emitted during the decay of the ^{229m}Th ions, neutralized by a graphene foil [22]. This

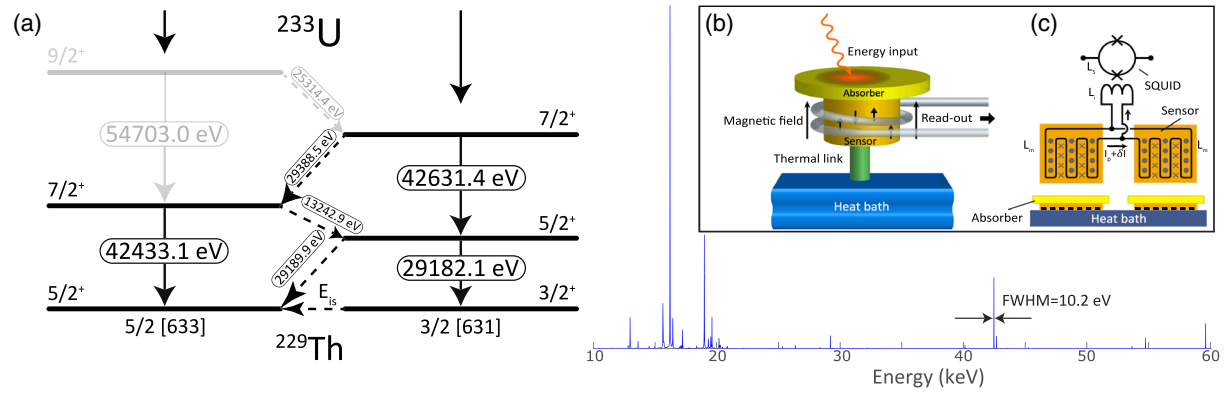

FIG. 1. (a) Partial nuclear level scheme of the ^{229}Th nucleus with relevant decay paths and energies. The nuclear states are grouped into two rotational bands, which are labeled by their bandheads: $5/2$ [633] (ground state) and $3/2$ [631] (isomeric state). The total spectrum in the energy range up to 60 keV is shown in the bottom. (b) Schematic of a magnetic microcalorimeter. A γ ray is absorbed in a gold absorber. The heat is then transferred and measured by a Ag:Er^{3+} paramagnetic sensor. A weak thermal link to the heat bath enables thermalization. (c) A persistent current (I_p) circulates in the superconducting meander-shaped pickup coil polarizing the magnetic moment in the sensor. As the flux in a superconducting loop is conserved, a change of flux $\Delta\Phi$ driven by a temperature-induced change of magnetization induces an additional screening current (δI), which is read out as a voltage drop over the dc-SQUID.

value was deduced by combining spectroscopy data of conversion electrons with calculated distributions of initial/final electronic states. The calculated uncertainty of the initial/final electronic state distribution significantly contributes to the uncertainty of the reported isomer energy (0.16 eV).

In the work presented here, we perform γ spectroscopy using the magnetic microcalorimeter (MMC) maXs-30. It is specially designed for optimal performance around 30 keV, corresponding to the weakest γ rays of interest produced in the $^{233}\mathrm{U} \rightarrow {}^{229}\mathrm{Th}$ α decay. This experiment complements the conversion electron experiment in that the isomer energy is extracted directly from the experimental data, without resorting to calculations. The only significant uncertainty in our experiment is the statistical error.

In magnetic microcalorimeters, the energy of a γ ray is converted into heat in a thin absorber plate [see Fig. 1(b)]. The absorbers used in this experiment are made of 20-μm thick gold layers, realizing 65% stopping efficiency at 30 keV while having 10 eV resolution. For a precise determination of the small temperature rise on the order of some hundred μK, MMCs make use of a paramagnetic temperature sensor operated in a weak magnetic field [32,33]. As a paramagnetic sensor, we use silver doped with a few hundred ppm of erbium.

The detector is composed of 8×8 pixels operated in pairs. Each pair of pixels consists of two gold absorbers, each read out by a Ag:Er^{3+} temperature sensor. Two parallel meander-shaped pickup coils made of niobium are connected to the input coil of a dc-SQUID current sensor. The pickup coils of the two sensors generate opposing currents for an equivalent magnetization change in the two sensors. The resulting screening current (δI) in the input coil of the dc-SQUID is directly proportional to the temperature difference of the two sensors. We read out the screening current as a linearized voltage drop over the dc-SQUID [see Fig. 1(c)] [34].

The γ radiation is emitted from a solution containing ^{233}U. Uranium is dissolved in an aqueous solution as uranyl nitrate $UO_2(NO_3)_2$ and is contained inside a polyether ether ketone (PEEK) capsule. The wall thickness of 2 mm shields α and β radiation but is transparent for photons above few keV. The activity of the source was 74 MBq. It was chemically purified at the Institute for Nuclear Chemistry, Johannes Gutenberg University Mainz, to remove daughter products of the uranium chain (Th, Ra, Ac) which increase the activity and hence background in the measurement. α and γ spectroscopy (using Ge detectors) performed on the source indicate a 2% ^{234}U and a < 1 ppm ^{232}U contamination. Additionally, traces of ^{238,240,242}Pu, ^{241}Am, ^{237}Np were identified (see the Supplemental Material [35], which includes Refs. [36–38]).

The γ spectrum in the energy range 0–60 keV was recorded over about 640 pixel $\times$ days, which corresponds to about 8 million events. For each absorption event, we recorded the full pulse shape, which shows a 9.6 μs fast voltage increase, followed by a $\tau = 2.7$ ms decay (see the Supplemental Material [35]). After every event, an electronic hold-off of 450 ms is used to allow for the thermalization of the detector and avoiding pileups. A single pulse amplitude value U is extracted for each event by fitting an amplitude-scaled pulse template [39]. This pulse template fitting allows to filter-out events, like a triggered pulse, with a pulse on the tail, which would otherwise distort the spectral shape. Events that occur within the signal rise time cannot be filtered. In the regions of interest, they produce a flat background, which does not affect the presented analysis.

The raw amplitude data obtained from each pixel are corrected for temperature, which is extracted from the

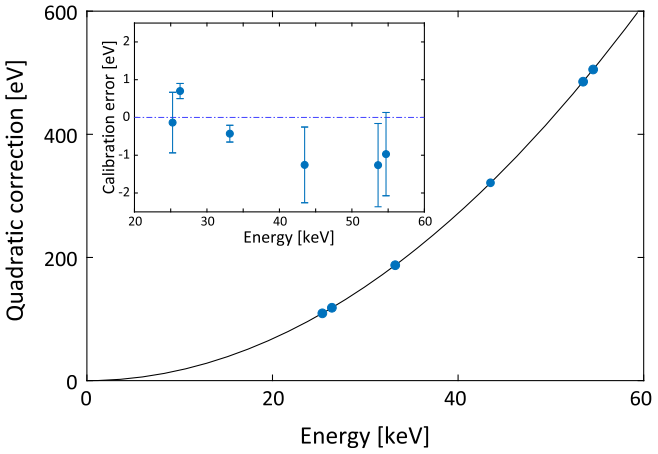

FIG. 2. Residual uncertainty of the calibration lines with respect to the literature values (see Table I) before the quadratic correction. The residuals follow the quadratic polynomial, indicating that quadratic correction is sufficient. Inset: residual energy differences after the quadratic correction. The standard deviation of the residual error is 0.76 eV.

simultaneously triggered asymmetric pixel pairs located in each of the four corners of the detector (see the Supplemental Material [35]). The data from individual pixels (p) are corrected quadratically $E(p) = a(p) \times (U(p) + b(p)U^2(p))$ to account for small differences in the individual pixel's gain characteristics and combined into a single data set E [40]. The maXs-30 shows an excellent gain linearity with a nonlinearity of only 0.60(2)% in the energy range of interest, i.e., up to 40 keV (see Fig. 2). A second-order polynomial with only a single fit parameter was sufficient to reduce the calibration-line residuals below 1.3 eV (see Fig. 2).

To use all the information available in the spectrum and to minimize the free parameters used in the energy calibration, the quadratic terms $b(p)$ are extracted directly from the experimental data. From energy conservation within the nuclear level structure, we identified two decay loops: 54.7 keV = 25.3 keV + 29.4 keV and 54.7 keV + 13.2 keV = 25.3 keV + 42.6 keV [see Fig. 1(a)]. The quadratic terms $b(p)$ are adjusted to self-consistently fulfill the two conditions above (see the Supplemental Material [35]).

To convert from the amplitude U to energy E, we use the reference lines listed in Table I. Experimentally, the linear correction terms for every pixel $a(p)$ are determined by minimizing the squares of the residuals, with the calibration points weighted by the fit and the literature uncertainties (see Fig. 2). For the calibration, we have chosen only well-resolved gamma lines. We excluded the ^{229}Th lines that are used in further data analysis and x-ray lines because their energy and line shape might be influenced by the chemical environment [41]. Three out of four energy calculations schemes used below are insensitive to the energy calibration [see Eqs. (1)–(4)]. Either the difference of energy levels [Eqs. (2) and (3)] is used to extract the isomer energy, or their line shape is analyzed using Eq. (1). However, the absolute energy scheme using Eq. (4) is sensitive to the energy calibration, and a different choice of calibration lines can lead to a different result.

Experimental imperfections, i.e., nonlinearities in the analog-to-digital conversion or detector chip inhomogeneity, can lead to small oscillations of the residuals of the energy calibration curve. These are too small to be quantified experimentally (see Fig. 2). We use the standard deviation of calibration lines from their literature values to estimate the uncertainty due to the local calibrations. The calibration uncertainty of every peak is 0.76 eV.

While higher-order nonlinearities contribute to the uncertainty of each peak's absolute energy, there is one more artifact affecting the line shapes that we have to consider during data analysis. The electronic signal after the photon absorption decays faster than the temperature of the pixel. This is caused by a differential readout of the pixel pairs and design details of the pairwise heat sinking of pixels [33,46]. If a new event occurs in the pixel pair before it cooled down to idle state, the signal response to energy input is reduced, leading to a reduced signal height, and low-energy tails in the spectrum. We mitigated this effect during the experiment by applying the hold-off mentioned above, but small distortions from a Gaussian line shape are still present.

To adequately describe the data, we use a generic line shape based on an asymmetric Voigt profile (see the Supplemental Material) that can fit all the gamma lines in the spectrum. The Gaussian function, characterized by

TABLE I. Reference lines used in the calibration. The uncertainty for measured values is dominated by the calibration uncertainty (0.76 eV). The contribution of the statistical uncertainty of the fit is negligible. The deviation from the literature values is reported as the number of standard deviations from the reference values (Resid. [σ]).

Decay path	Measured	Reference	Resid. [σ]	Ref.
^{229}Th$(9/2^+ \rightarrow 7/2^+)$	25314.4(8)	25314.6(8)	0.2	[29]
^{237}Np$(5/2^- \rightarrow 7/2^+)$	26345.3(8)	26344.6(2)	3.4	[42]
^{237}Np$(7/2^+ \rightarrow 5/2^+)$	33195.8(8)	33196.3(2)	2.2	[43]
^{234}U$(2^+ \rightarrow 0^+)$	43496.8(8)	43498.1(10)	1.3	[44]
^{229}Th$(9/2^+ \rightarrow 7/2^+)$	53609.3(8)	53610.7(11)	1.2	[29]
^{229}Th$(9/2^+ \rightarrow 7/2^+)$	54703.0(8)	54704.0(11)	0.9	[45]

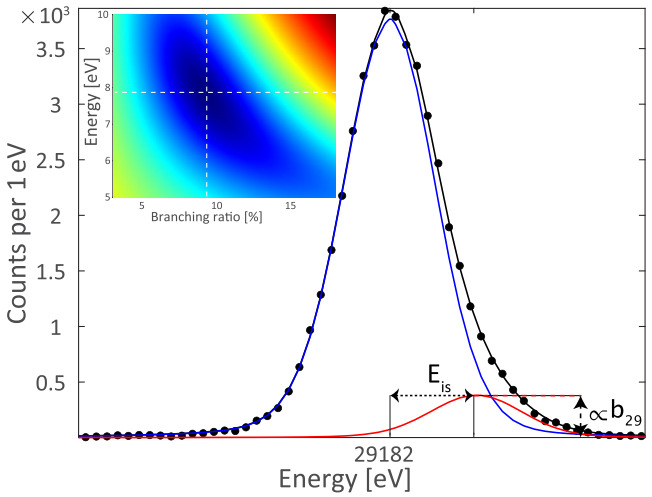

FIG. 3. Line shape of the 29.2 keV doublet. The red curve represents the fit of the 29 190 eV line, and the blue curve represents the fit of the 29 182 eV line. The branching ratio b_{29} and the isomer energy (E_{is}) can be extracted directly from this fit. The inset shows a two-dimensional plot of χ^2 as a function of branching ratio and the isomer energy. The white dashed lines point to the fitted E_{is} and b_{29} values.

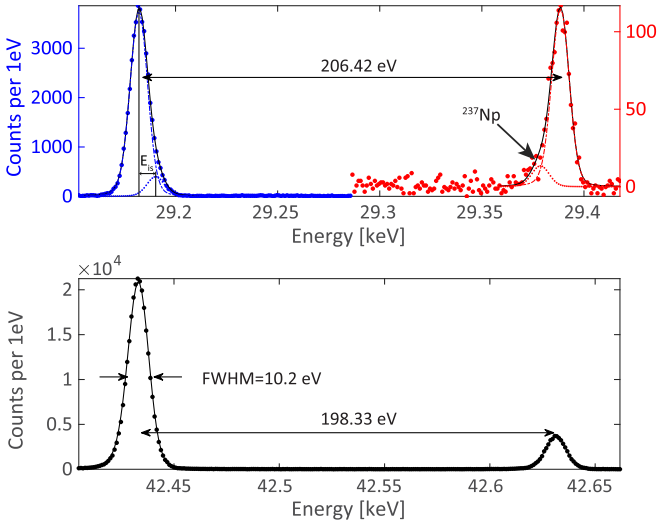

FIG. 4. MMC spectra of the 29 and 42 keV doublets. The ^{237}Np contamination leads to a weak signal [29378.6(18) eV] which overlaps the 29.4 keV line (see the Supplemental Material [35]).

variance (σ), is convolved with a wider Lorentzian profile on the low-energy side (γ_1) and a narrower Lorentzian profile on the high-energy side (γ_2). All three parameters follow a weak quadratic dependence on the energy of the line $\sigma = \sigma^0(1 + cE^2)$ and $\gamma_{1(2)} = \gamma^0_{1(2)}(1 + cE^2)$. These four parameters $(\sigma, \gamma_1, \gamma_2, c)$ were extracted from a simultaneous fit of all γ lines; they are common to all the γ lines in the spectrum. For each individual line fit, only two free parameters are varied, the amplitude (A) and the energy (E).

The energy resolution of ~10 eV [see Fig. 1(a)] together with the outstanding linearity (see Fig. 2) of the maXs-30 microcalorimeter allows us to perform four different types of data analysis to extract the ^{229}Th isomer energy. With high resolution, we can partly resolve the 29.2 keV doublet line (see Fig. 3). By analyzing its line shape deviations compared to isolated lines in the spectrum, we can extract both the isomer energy (E_{is}) and the branching ratio (b_{29}). To analyze the line doublets, we use a pair of generic line shapes from Fig. 4 and let the doublet splitting and their relative amplitudes as free parameters. From their relative amplitudes, we measure that the $5/2^+$ state has a significant interband decay probability of $b_{29} = 9.3(6)\%$, which leads to a doublet shape of the 29.2 keV line with a splitting equal to the isomer energy [see Fig. 1(a)]. We find a value of

$$E_{\mathrm{is,line\ shape}} = 7.84(29)\ \mathrm{eV}. \tag{1}$$

The 42.4 keV line shows a very small line shape deviation from a monoenergetic line. This allowed us to put an upper one-sigma bound on the branching ratio $b[(42.4\mathrm{keV}\to 8\mathrm{eV})/(42.4\mathrm{keV}\to 0\mathrm{eV})] = b_{42} < 0.7\%$. These branching ratios are consistent with the previous experimental value for $b_{29} = 9.3(6)\%$ [27], and b_{42} lies in the range of theoretical predictions $0.2\% < b_{42} < 2\%$ [47]. There is a strong correlation between the $E_{\mathrm{is,line\ shape}}$ and b_{29}. A more accurate independent measurement of b_{29} combined with our experiment would further decrease the uncertainty of the isomer energy.

The second analysis makes use of the two pairs of closely spaced lines at 29 and 42 keV. Measuring the distances of these two pairs yields (E_{is}) (see Fig. 4). A previous experiment performed with a silicon semiconductor microcalorimeter extracted E_{is} using this scheme, however, with a much higher uncertainty due to the limited resolution and higher nonlinearities [23,24].

The absolute energy scheme uncertainty of each peak is dominated by the calibration uncertainty (0.76 eV). Because the calibration uncertainty is a slowly varying function of the energy, it is significantly compensated when subtracting energies of closely spaced lines ΔE_{29} and ΔE_{42} (see Fig. 4). The lines 29.18 and 42.43 keV, due to their doublet nature, are fitted with two generic line shapes each. The relative amplitudes of these functions are set according to known interband branching ratios and the spacing is E_{is} (see the Supplemental Material [35]). The interband branching ratios are $b_{29} = 9.3(6)\% = [1/9.8(6)]$ and $b_{42} = 0.3(3)\% = 1/305$ [24,27].

We obtain the isomer energy as

$$E_{\mathrm{is},1} = 206.42(17)\ \mathrm{eV} - 198.33(2)\ \mathrm{eV} = 8.10(17)\ \mathrm{eV}. \tag{2}$$

The uncertainty emerges from the statistics of the weak 29.4 keV line (0.12 eV), from the uncertainty of the branching ratio (0.03 eV), and from the uncertainty of

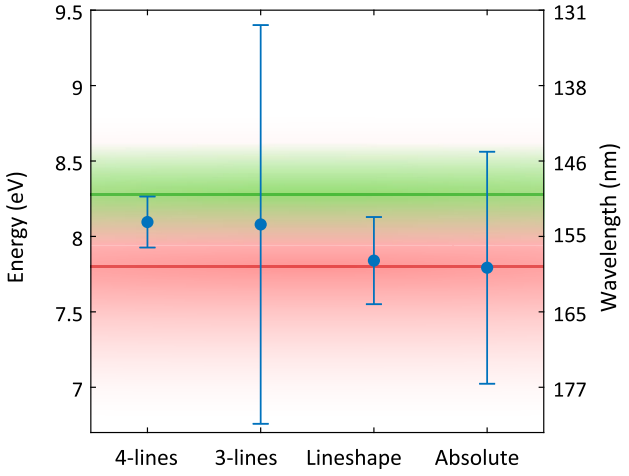

FIG. 5. Isomer energies E_{is} measured in this study compared to previous experiments using γ spectroscopy. The green and red faded areas represent the isomer energy reported in [22,24], respectively, with their corresponding uncertainties. Error bars for our E_{is} represent the root sum square of statistical and systematic uncertainty.

the ^{237}Np contamination (0.12 eV); see the Supplemental Material [35].

Alternatively, we can extract the isomer energy as

$$E_{is,2} = 42433.1\,\text{eV} - 13242.9\,\text{eV} - 29182.1\,\text{eV} = 8.1(13)\,\text{eV}. \tag{3}$$

This method has the advantage of avoiding the weak interband 29.4 keV transition [see Fig. 1(a)]. The disadvantage is that there are no closely spaced line pairs. Therefore, the calibration uncertainty is not compensated but adds up. This result is consistent with the analysis of Eq. (2), but the uncertainty is much higher (see Fig. 5).

In a recent experiment, synchrotron radiation was used to excite the ground state of ^{229}Th to the $(5/2^+)$ state (interband transition), the excitation energy was measured as 29 189.93(7) eV [27]. In this work, we have accurately measured the intraband transition from the $(5/2^+)$ state to the isomer state: 29 182.1(8) eV (see Fig. 1). Subtracting these two values yields a fourth value for E^{is},

$$E_{is,abs} = 29189.93(7)\ \text{eV} - 29182.1(8)\ \text{eV} = 7.8(8)\ \text{eV}. \tag{4}$$

The estimated uncertainty is dominated by the calibration uncertainty (0.76 eV). This scheme was recently used in another experiment, reporting an isomer energy of $[E_{is} = 8.30(92)\ \text{eV}]$ [25].

In conclusion, the energy of the ^{229}Th isomer state was measured by recording a high resolution (FWHM $\approx$ 10 eV) high bandwidth ($\sim$60 keV) γ spectrum using a cryogenic magnetic microcalorimeter. We extracted the isomer energy using four different schemes. A comparison of all four results with previous experiments is summarized in Fig. 5. Weighting these results with their statistical and systematic uncertainty and combining them, we constrain the one-sigma interval for the isomer energy to be $7.88\ \text{eV} < E_{is} < 8.16\ \text{eV}$. We also measured the branching ratio of the second excited state $b_{29} = 9.3(6)\%$ and found it to be compatible with previously measured values.

This work was supported by the European Union's Horizon 2020 research and innovation program under Grant No. 664732 "nuClock," Grant No. 856415 "ThoriumNuclearClock," Grant No. 882708 "CrystalClock," and Grant No. 824109 "European Microkelvin Platform." The project has also received funding from the European Metrology Program For Innovation And Research (EMPIR) program co-financed by the participating states and from the European Union's Horizon 2020 research and innovation program. We thank N. Trautmann for his contributions to the source preparation and the staff of the mechanical workshop of the Institute of Nuclear Chemistry in Mainz for the construction of the ^{233}U liquid-source container, J. Schwestka for sample preparation at TU Wien, and S. Stellmer and P. Thirolf for helpful discussions.

*T. S. and J. G. contributed equally to this work.

[1] P. G. Thirolf, B. Seiferle, and L. von der Wense, J. Phys. B **52**, 203001 (2019).
[2] E. Peik and M. Okhapkin, C. R. Phys. **16**, 516 (2015).
[3] E. V. Tkalya, Phys. Rev. Lett. **106**, 162501 (2011).
[4] E. Peik and C. Tamm, Europhys. Lett. **61**, 181 (2003).
[5] C. J. Campbell, A. G. Radnaev, A. Kuzmich, V. A. Dzuba, V. V. Flambaum, and A. Derevianko, Phys. Rev. Lett. **108**, 120802 (2012).
[6] W. G. Rellergert, D. DeMille, R. R. Greco, M. P. Hehlen, J. R. Torgerson, and E. R. Hudson, Phys. Rev. Lett. **104**, 200802 (2010).
[7] G. A. Kazakov, A. N. Litvinov, V. I. Romanenko, L. P. Yatsenko, A. V. Romanenko, M. Schreitl, G. Winkler, and T. Schumm, New J. Phys. **14**, 083019 (2012).
[8] V. V. Flambaum, Phys. Rev. Lett. **97**, 092502 (2006).
[9] J. C. Berengut and V. V. Flambaum, Nucl. Phys. News **20**, 19 (2010).
[10] P. Thirolf, B. Seiferle, and L. Von der Wense, Ann. Phys. (Amsterdam) **531**, 1970022 (2019).
[11] Y. V. Stadnik and V. V. Flambaum, Phys. Rev. A **94**, 022111 (2016).
[12] A. Arvanitaki, J. Huang, and K. Van Tilburg, Phys. Rev. D **91**, 015015 (2015).
[13] S. Kolkowitz, I. Pikovski, N. Langellier, M. D. Lukin, R. L. Walsworth, and J. Ye, Phys. Rev. D **94**, 124043 (2016).
[14] M. Bondarescu, R. Bondarescu, P. Jetzer, and A. Lundgren, EPJ Web Conf. **95**, 04009 (2015).
[15] *Proceedings of the 30th International Technical Meeting of the Satellite Division of the Institute of Navigation* (Portland, OR, 2017).
[16] L. von der Wense, B. Seiferle, and P. G. Thirolf, Meas. Tech. **60**, 1178 (2018).

[17] J. Jeet, C. Schneider, S. T. Sullivan, W. G. Rellergert, S. Mirzadeh, A. Cassanho, H. P. Jenssen, E. V. Tkalya, and E. R. Hudson, Phys. Rev. Lett. **114**, 253001 (2015).
[18] A. Yamaguchi, H. Muramatsu, T. Hayashi, N. Yuasa, K. Nakamura, M. Takimoto, H. Haba, K. Konashi, M. Watanabe, H. Kikunaga, K. Maehata, N. Y. Yamasaki, and K. Mitsuda, Phys. Rev. Lett. **123**, 222501 (2019).
[19] S. Stellmer, G. Kazakov, M. Schreitl, H. Kaser, M. Kolbe, and T. Schumm, Phys. Rev. A **97**, 062506 (2018).
[20] L. Kroger and C. Reich, Nucl. Phys. **A259**, 29 (1976).
[21] L. von der Wense, B. Seiferle, M. Laatiaoui, J. B. Neumayr, H.-J. Maier, H.-F. Wirth, C. Mokry, J. Runke, K. Eberhardt, Ch. E. Düllmann, N. G. Trautmann, and P. G. Thirolf, Nature (London) **533**, 47 (2016).
[22] B. Seiferle, L. von der Wense, P. V. Bilous, I. Amersdorffer, C. Lemell, F. Libisch, S. Stellmer, T. Schumm, Ch. E. Düllmann, A. Pálffy, and P. G. Thirolf, Nature (London) **573**, 243 (2019).
[23] B. R. Beck, J. A. Becker, P. Beiersdorfer, G. V. Brown, K. J. Moody, J. B. Wilhelmy, F. S. Porter, C. A. Kilbourne, and R. L. Kelley, Phys. Rev. Lett. **98**, 142501 (2007).
[24] B. Beck, C. Wu, P. Beiersdorfer, G. Brown, J. Becker, K. Moody, J. Wilhelmy, F. Porter, C. Kilbourne, and R. Kelley, *12th International Conference on Nuclear Reaction Mechanisms* (2009), lLNL-PROC-415170.
[25] A. Yamaguchi, H. Muramatsu, T. Hayashi, N. Yuasa, K. Nakamura, M. Takimoto, H. Haba, K. Konashi, M. Watanabe, H. Kikunaga, K. Maehata, N. Y. Yamasaki, and K. Mitsuda, Phys. Rev. Lett. **123**, 222501 (2019).
[26] B. Seiferle, L. von der Wense, and P. G. Thirolf, Phys. Rev. Lett. **118**, 042501 (2017).
[27] T. Masuda *et al.*, Nature (London) **573**, 238 (2019).
[28] L. Kroger and C. Reich, Nucl. Phys. **259A**, 29 (1976).
[29] R. G. Helmer and C. W. Reich, Phys. Rev. C **49**, 1845 (1994).
[30] Z. O. Guimarães-Filho and O. Helene, Phys. Rev. C **71**, 044303 (2005).
[31] J. Thielking, M. V. Okhapkin, P. Glowacki, D. M. Meier, L. von der Wense, B. Seiferle, Ch. E. Düllmann, P. G. Thirolf, and E. Peik, Nature (London) **556**, 321 (2018).
[32] A. Fleischmann, C. Enss, and G. M. Seidel, Metallic magnetic calorimeters, in *Cryogenic Particle Detection*, edited by C. Enss (Springer, Berlin, Heidelberg, 2005), pp. 151–216.
[33] A. Fleischmann, L. Gastaldo, S. Kempf, A. Kirsch, A. Pabinger, C. Pies, J. P. Porsf, P. Ranitzsch, S. Schäfer, F. V. Seggern, T. Wolf, C. Enss, and G. M. Seidel, AIP Conf. Proc. **1185**, 571 (2009).
[34] S. Kempf, M. Wegner, L. Deeg, A. Fleischmann, L. Gastaldo, F. Herrmann, D. Richter, and C. Enss, Supercond. Sci. Technol. **30**, 065002 (2017).
[35] See Supplemental Material at http://link.aps.org/supplemental/10.1103/PhysRevLett.125.142503 for the RAW data repository and additional information about sample contamination, signal processing, detector anatomy, energy calibration, self-consistent isomer energy calculation, and generic lineshape.
[36] D. Hengstler, Development and characterization of two-dimensional metallic magnetic calorimeter arrays for the high-resolution x-ray spectroscopy, Ph.D. thesis, Heidelberg University, 2017.
[37] S. Kempf, A. Ferring, A. Fleischmann, and C. Enss, Supercond. Sci. Technol. **28**, 045008 (2015).
[38] J. Geist, Determination of the isomer energy of ^{229}Th with the high-resolution micro-calorimeter array maXs30, Ph.D. Thesis, Heidelberg University, 2020.
[39] C. Enss, A. Fleischmann, K. Horst, J. Schönefeld, J. Sollner, J. S. Adams, Y. H. Huang, Y. H. Kim, and G. M. Seidel, J. Low Temp. Phys. **121**, 137 (2000).
[40] C. R. Bates, C. Pies, S. Kempf, D. Hengstler, A. Fleischmann, L. Gastaldo, C. Enss, and S. Friedrich, Appl. Phys. Lett. **109**, 023513 (2016).
[41] J. Campbell, Nucl. Instrum. Methods Phys. Res., Sect. B **49**, 115 (1990).
[42] R. G. Helmer and C. Van der Leun, Nucl. Instrum. Methods Phys. Res., Sect. A **450**, 35 (2000).
[43] M. Basunia, Nucl. Data Sheets **107**, 2323 (2006).
[44] E. Browne and J. Tuli, Nucl. Data Sheets **108**, 681 (2007).
[45] V. Barci, G. Ardisson, G. Barci-Funel, B. Weiss, O. El Samad, and R. K. Sheline, Phys. Rev. C **68**, 034329 (2003).
[46] A. G. Kozorezov, C. J. Lambert, S. R. Bandler, M. A. Balvin, S. E. Busch, P. N. Nagler, J.-P. Porst, S. J. Smith, T. R. Stevenson, and J. E. Sadleir, Phys. Rev. B **87**, 104504 (2013).
[47] E. V. Tkalya, C. Schneider, J. Jeet, and E. R. Hudson, Phys. Rev. C **92**, 054324 (2015).